Indian Journal of Pure & Applied Physics
Vol. 63, February 2025, pp. 132-143
DOI: 10.56042/ijpap.v63i2.15219

Determination of X-ray Photon Absorption Properties of Some Human Tissues and Organs Using Monte Carlo method

Hasan Gulbicim[a*], Huseyin Akan[b] & Mustafa Cagatay Tufan[c]

[a]Ondokuz Mayıs University, School of Medicine, Department of Nuclear Medicine, 55200, Samsun, Turkey
[b]Ondokuz Mayıs University, School of Medicine, Department of Radiology, 55200, Samsun, Turkey
[c]Ondokuz Mayıs University, Graduate School, Department of Radiological Sciences, 55200, Samsun, Turkey

Received 21 November 2024; accepted 27 January 2025

The interaction of photons with human tissues and organs is a critical area of study for healthcare professionals and medical physicists. This study investigates the photon absorption properties of various tissues and organs, across a broad energy range, with a particular focus on the X-ray energy range emitted from the Computed Tomography (CT) devices. The mass attenuation coefficient (μ_m), linear attenuation coefficient (μ), total atomic cross-section ($\sigma_{t,a}$), total electronic cross-section ($\sigma_{t,e}$), effective atomic number (Z_{eff}), effective electron density (N_{eff}), half-value layer (HVL), tenth-value layer (TVL), and mean free path (MFP)were calculated through an improved user code developed for this study. The results were compared to data obtained from the XCOM database, and showed excellent agreement, validating the accuracy of the method. In addition, the variations in radiation dose depending on the depth in some tissues and organs are also shown in this study. This comprehensive study provides a unique dataset for these radiation interaction quantities, which has not been collectively presented in previous literature. Our findings are expected to significantly enhance the understanding of photon interactions with human tissues and organs, particularly within the context of medical imaging and therapeutic applications.

Keywords: X-ray; Absorption; Human tissue/organs; Monte carlo; XCOM

1 Introduction

With recent advancements in technology, the application areas and utilization of ionizing radiation in medicine are gradually increasing for diagnosing and treating diseases in departments such as nuclear medicine, radiation oncology, and radiology. Due to its non-invasive nature, various imaging modalities have also become an integral part of many other medical branches. As a result, it is well-known that many individuals, including patients, radiation workers, and specialists, are significantly exposed to ionizing radiation, due to the growing use of radiation emitting-devices. Moreover, it is also known that different tissues and organs in the human body show varying levels of sensitivity to such exposure. Therefore, it is crucial to have precise and detail knowledge of the physical interactions between target organs and radiation across various photon energy levels, including specific low, medium, and high energy regions. This is essential for understanding the impacts of receiving radiation dose and ensuring the safety of living organs.

Corresponding author: (E-mail:hasanglbcm@gmail.com)

The comprehensive understanding of interaction mechanisms of radiation with human organs requires determining various physical quantities. These quantities are derived from the attenuation of photons as they pass through the sample. The first one is the linear attenuation coefficient (μ), which is the fundamental quantity that generates image formation and provides tissue contrast in diagnostic modalities. Its value physically depends on both sample density and photon energy. To evaluate tissues and organs relative to each other, regardless of their density, a distinct quantity is required. In this context, the mass attenuation coefficient (μ_m) is the most frequently used one, which is obtained by dividing the linear attenuation coefficient with sample density. The interaction probabilities between radiation and the matter depend on the atomic ($\sigma_{t,a}$) and electronic ($\sigma_{t,e}$) interaction cross-sections, effective atomic number (Z_{eff}), and effective electron density (N_{eff}). In addition to these quantities, Half-Value Layer (HVL), Tenth-Value Layer (TVL), and Mean Free Path (MFP) are useful quantities for evaluating the macroscopic behavior of radiation in tissue.

Upon reviewing the literature on this subject since last two decades, several significant studies have been

identified. Most of them have only focused on calculating the mass attenuation coefficients for various tissues and tissue substitutes[1-17]. Effective atomic numbers for various tissues have also been calculated by several researchers[18-21]. Several studies have computed energy absorption build-up factors[22-26]. Effective electron densities for various tissues have also been determined by the authors in Refs[2,20] using Auto-Z_{eff} and WinXCom program. Linear attenuation coefficients have been investigated for various tissue substitutes and some other materials[27,28]. Unlike the majority of mentioned studies, some researchers have conducted studies with different focuses. In these studies, a simple Monte Carlo algorithm was developed to create bone composition models for dose calculations[29], while photon scattering cross-sections for cortical bone tissue were computed at diagnostic energy values[30].

The aim of this study is to determine photon absorption quantities and dose variations depending on tissue depth for various human tissues and organs across in a wide photon energy range, with a particular focus on X-rays emitted from computed tomography (CT). This will enable specialists, including physicians, medical physicists, and radiation workers, to access comprehensive photon absorption quantities for various tissues and organs, especially in the CT X-ray energy. Consequently, these professionals will be able to easily perform microscopic and macroscopic evaluations of the interactions between radiation and the respective tissues and organs. To determine the radiation absorption quantities and dosimetric changes for tissues and organs, the EGSnrc simulation code[31] was preferred due to its reliability in modeling the interaction of radiation with matter.The results calculated by EGSnrc were also compared to those obtained from the National Institute of Standards and Technology's (NIST) XCOM database[32].

2 Materials and Methods

2.1 Photon Absorption Quantities

The photon absorption properties of a given sample are fundamentally based on the exponential absorption law, known as Lambert-Beer law[11], and several crucial quantities derived from it. One of the most important quantities is the linear attenuation coefficient, which is derived from the following equation:

$$I = I_0 e^{-\mu x} \quad \text{... (1)}$$

where I_0, I, *x* and μ are the photon intensity at the surface of the medium, photon intensity at *x,* sample thickness and the linear attenuation coefficient which is depend on the photon energy and sample density[33], respectively. The mass attenuation coefficient is a crucial parameter for describing the absorption properties of radiation in a sample and determined by dividing the linear attenuation coefficient to the density of the sample. For a compound or mixture, it is calculatedby the following equation:

$$\mu_m = \sum_i w_i \left(\frac{\mu}{\rho}\right)_i \quad \text{... (2)}$$

Where w_i, μ_i and ρ_i represent the weight fraction, linear attenuation coefficient and the density of the ith element in the sample, respectively[34]. The mass attenuation coefficient also allows for the calculation of boththe atomic cross-section and electronic cross-section of multi element medium (compound or mixture) interacting with incoming photons. These quantities are expressed byequations 2 and 3, respectively.

$$\sigma_{t,a} = \frac{\mu_m N}{N_A} \quad \text{... (3)}$$

$$\sigma_{t,e} = \frac{1}{N_A} \sum \frac{f_i N_i}{Z_i} (\mu_m)_i \quad \text{... (4)}$$

Here, N represents the atomic mass of the medium and N_A denotes the Avogadro's number. The symbol f_i denotes the fractional abundance of the ith element relative to the total number of atoms, ensuring that $\Sigma f_i = 1$, while Z_i and N_i indicate the atomic number and mass of the ith element, respectively[35].

The effective atomic number (Z_{eff}) and effective electron density (N_{eff}) are key quantities for understanding photon interactions with composite materials and biological tissues. Z_{eff}, a weighted average of atomic numbers, and N_{eff}, the number of electrons per unit mass, vary with photon energy and assist in dose estimation, tissue differentiation, and radiation shielding design. These quantities, essential in medical imaging and therapy, are related to $\sigma_{t,a}$ and $\sigma_{t,e}$ as shown in the following equations[35]:

$$Z_{eff} = \frac{\sigma_{t,a}}{\sigma_{t,e}} \quad \text{... (5)}$$

$$N_{eff} = \frac{N_A}{N} Z_{eff} \sum n_{i=} \frac{\mu_m}{\sigma_{t,e}} \quad \text{... (6)}$$

On the other hand, three key quantities -the half-value layer (HVL), tenth-value layer (TVL), and

mean free path (MFP)-provide a macroscopic evaluation of photon travel within tissues. The HVL (half-value layer) is the tissue thickness at which the incident photons are attenuated to half of their initial intensity, while the TVL (tenth-value layer) is the thickness where photons are attenuated to one-tenth, as indicated by Eqs. 7 and 8.

$$HVL = \frac{\ln(2)}{\mu} \quad \ldots (7)$$

$$TVL = \frac{\ln(10)}{\mu} \quad \ldots (8)$$

The MFP is the thickness of a medium that reduces the number of incident photon intensity 1/e (approximately 37%) of their initial number. This quantity represents the average distance that a photon travels within a medium and serves as a measure of the penetration power of a photon beam before it interacts[33]. This relationship is defined by Eq. 9 for mono-energetic photons.

$$MFP = \frac{1}{\mu} \quad \ldots (9)$$

2.2 EGSnrc Code

EGSnrc is an advanced Monte Carlo simulation toolkit for modeling ionizing radiation transport through matter, including photons, electrons, and positrons with energies from 1 keV to 10 GeV. EGSnrc, an advanced version of the Electron Gamma Shower (EGS) software originally developed at the Stanford Linear Accelerator Center (SLAC) in the 1970s, was extensively updated in 2000. These updates included enhanced algorithms for simulating multiple scattering, energy loss, and photon interactions, along with more accurate low-energy cross-section data[31]. The egs++ library enables complex geometry and source modeling, crucial for medical physics applications like radiation therapy dose calculations and imaging system design. EGSnrc supports custom material definitions and voxel-based geometries, ensuring high simulation accuracy. Its modular design, validated reliability, parallel processing capabilities, and active user community make it a powerful tool for applications in medical physics, radiation protection, and high-energy physics.

2.3 NIST's XCOM software

In this study, the validation of the obtained data was conducted using the NIST's XCOM software. The XCOM software, developed by the National Institute of Standards and Technology (NIST), is a vital tool in radiation physics and related disciplines. It provides crucial data on photon interaction cross-sections with matter across a broad energy spectrum from 1 keV to 100 GeV, encompassing processes such as photoelectric absorption, coherent and incoherent scattering, and pair production[32]. This data is fundamental for understanding photon behavior within a medium, influencing applications in medical physics, radiation protection, and material science. Initially developed to address the needs of radiation physics and dosimetry, XCOM has become a versatile tool used across various disciplines where photon interactions play a crucial role.

2.4 Simulation of photon transport

In this study, a customized user code was developed within the EGSnrc simulation toolkit, a general-purpose Monte Carlo code, to determine the photon absorption quantities of various tissues and organs. Narrow-beam geometry was preferred for photon transport in the Monte Carlo simulations. The simulation model implemented for the Monte Carlo calculations was shown in Fig. 1.

All produced photons in simulations were sent to the target from a single point in a straight line. A planar phantom geometry with various thicknesses, depending on photon energy, was utilized for modeling the target tissues and organs. A total of 11 different tissue/organ models and water were incorporated in this study. Each of them were defined with a unique realistic phantom content. The elemental compositions of the anatomical structures within the phantoms were taken from the ICRU Report-46[36] and from Ref[37]. Elemental compositions and mass densities of the tissues and organs used in this work are presented in Table 1.

Photon interaction cross-sections for the tissue and organs were computed using the PEGS4 software, a

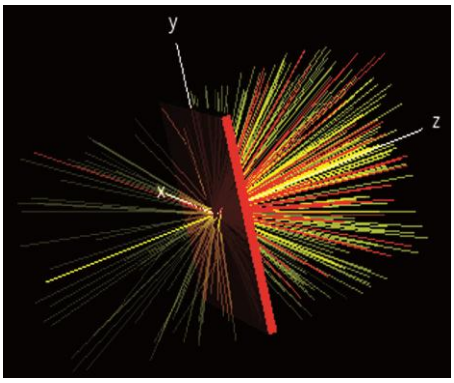

Fig. 1 — Monte Carlo simulation geometry used to determine the absorption quantities

Table 1 — Definitions of elemental compositions of tissues and organs utilized in MC calculations.

No	Tissue/Organ	Elemental compositions (%) of tissue and organs	Mass density (g/cm^3)
1	Fat	H: 0.114, C: 0.598, N: 0.007, O: 0.278, Na: 0.001, S: 0.001, Cl: 0.001	0.95
2	Soft tissue	H: 0.105, C: 0.256, N: 0.027, O: 0.602, Na: 0.001, P: 0.002, S: 0.003, Cl: 0.002, K: 0.002	1.03
3	Lung	H: 0.103, C: 0.105, N: 0.031, O: 0.749, Na: 0.002, P: 0.002, S: 0.003, Cl: 0.003, K: 0.002	0.26
4	Blood	H: 0.102, C: 0.110, N: 0.033, O: 0.745, Na: 0.001, P: 0.001, S: 0.002, Cl: 0.003, K: 0.002, Fe: 0.001	1.06
5	Muscle	H: 0.102, C: 0.143, N: 0.034, O: 0.710, Na: 0.001, P: 0.002, S: 0.003, Cl: 0.001, K: 0.004	1.04
6	Brain (Gray and white matter)	H: 0.107, C: 0.145, N: 0.022, O: 0.712, Na: 0.002, P: 0.004, S: 0.002, Cl: 0.003, K: 0.003	1.03
7	Eye lens	H: 0.096, C: 0.195, N: 0.057, O: 0.646, Na: 0.001, P: 0.001, S: 0.003, Cl: 0.001	1.07
8	Cortical bone	H: 0.034, C: 0.155, N: 0.042, O: 0.435, Na: 0.001, P: 0.103, Mg: 0.002, S: 0.003, Ca: 0.225	1.92
9	Compact bone	H: 0.064, C: 0.278, N: 0.027, O: 0.410, P: 0.070, S: 0.002, Mg: 0.002, Ca: 0.147	1.85
10	Skin	H: 0.101, C: 0.228, N: 0.046, O: 0.619, S: 0.002, K: 0.001	1.10
11	Liver	H: 0.102, C: 0.139, N: 0.030, O: 0.716, Na: 0.002, P: 0.003, S: 0.003, Cl: 0.002, K: 0.003	1.06
12	Water	H: 0.112, O: 0.888	1.00

user code defining media data for EGSnrc. During the simulation, cut-off energies for electron and photon transport were set as 10 keV and 5 MeV, respectively. To obtain accurate results and minimize statistical errors, the simulations were carried out by 2×10^8 photon histories. Some photons pass through the sample without any interaction, while others scatter backward or forward at lower energies and various angles through coherent and incoherent scattering with the atomic electrons of the target sample. Additionally, some simulated photons are completely absorbed through photoelectric absorption within the target medium. During these interactions, atomic electrons can be ejected from their orbits, and these ejected electrons are demonstrated in red as shown in Fig. 1. Following this entire process, the linear attenuation coefficients of the samples are determined using Eq. 1.

3 Results and Discussion

3.1 Photon absorption properties of tissue and organs

In this section, key quantities representing the radiation absorption properties of 11 different human tissues, organs, and water were presented. These quantities were calculated using both the EGSnrc code and XCOM software.The mass attenuation coefficients, linear attenuation coefficients, HVL, TVL, and MFP values were calculated using EGSnrc for photon energies between 0.02 and 2.0 MeV, while Z_{eff}, N_{eff}, $\sigma_{t,a}$ and $\sigma_{t,e}$, were calculated for photon energies between 0.02 and 5.0 MeV. In addition, all of these quantities were calculated using XCOM across a broader photon energy range of 0.01 to 10^4 MeV to observe their behavior over a wider energy range. So, Figs. 2 - 9 illustrate these quantities within this extended energy range.

Noticeable differences can be observed in the mass attenuation coefficients of tissues and organs across photon energies within and below the circled region as shown in Fig. 2. In this energy region, the mass attenuation coefficient strongly depends on the atomic number of the elements comprising the medium. The K and L shell edges are also visible in this graph within the energy range of 5 to 10 keV for compact bone and cortical bone tissues, as these tissues have higher atomic numbers compared to the others. Between 0.150 MeV and 10 MeV, the mass attenuation coefficients of tissues and organs decrease at nearly the same rate and similar values as photon energy increases. Above 10 MeV, noticeable differences in the mass attenuation coefficients among tissues and organs are also observed, which are directly related with the atomic number of the medium.

To compare our findings and XCOM results, the calculated mass attenuation and linear attenuation coefficients of soft tissue are given in Table 2 covering the photon energy range of 0.02 to 2.0 MeV. Within this range, particular attention is given to the interval between 0.02 and 0.140 MeV, as it is commonly utilized in medical applications and

Table 2 — The calculated mass attenuation and linear attenuation coefficients of soft tissue.

Energy (MeV)	*This study* μ (cm^{-1})			*This study* μ_m (cm^2/g)		*Rafiei et al.* [15] μ_m (cm^2/g)	*Salehi et al.* [24] μ_m (cm^2/g)
	XCOM	EGSnrc	Diff.%	XCOM	EGSnrc	MCNPX	GP-FIT
0.020	0.6983	0.6996	0.1767	0.6780	0.6792		0.7616
0.040	0.2422	0.2437	0.6340	0.2351	0.2366		0.0683
0.060	0.1959	0.1966	0.3667	0.1902	0.1909		0.0304
0.080	0.1795	0.1794	-0.0574	0.1743	0.1742		0.0241
0.100	0.1692	0.1689	-0.1829	0.1643	0.1640	0.1685	0.0233
0.120	0.1613	0.1607	-0.3846	0.1566	0.1560		
0.140	0.1546	0.1551	0.3320	0.1501	0.1506		
0.364	0.1123	0.1122	-0.0918	0.1090	0.1089		
0.662	0.0877	0.0876	-0.1176	0.0851	0.0850		
1.000	0.0723	0.0725	0.2841	0.0702	0.0704	0.0700	0.0700
1.250	0.0647	0.0646	-0.1595	0.0628	0.0627		
1.500	0.0588	0.0588	0.0000	0.0571	0.0571		0.0570
2.000	0.0506	0.0505	-0.2041	0.0491	0.0490		0.0489

t-test: 0.0032 p-value: 0.9974 (0.0025: << 0.05)

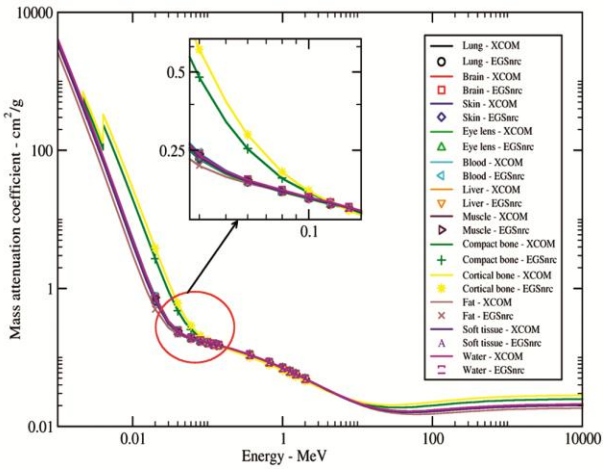

Fig. 2 — Variations in the mass attenuation coefficients of tissues and organs calculated by EGSnrc and XCOM. The circled region encompasses the photons emitted from Computed Tomography

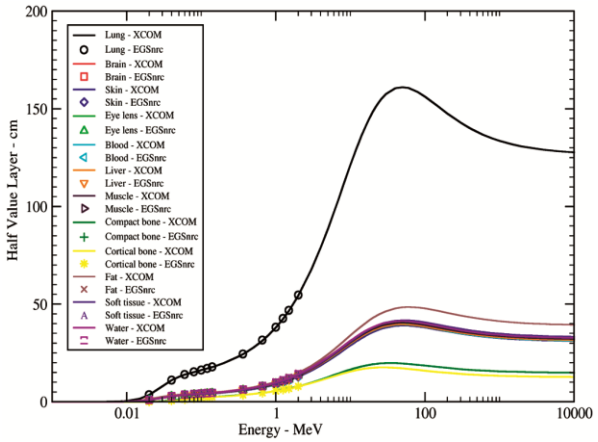

Fig. 3 — HVL variations of tissues and organs across photon energies using EGSnrc and XCOM

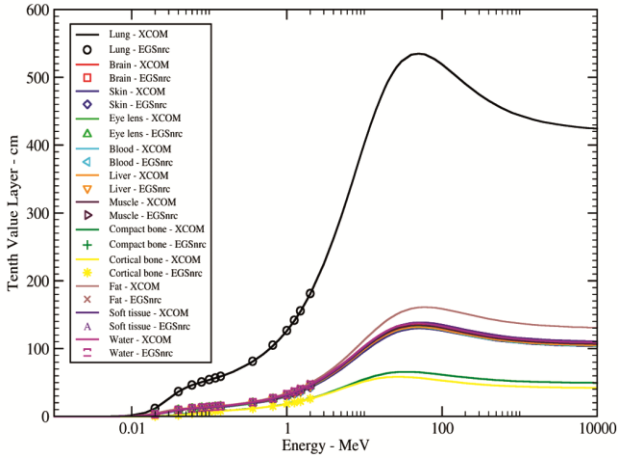

Fig. 4 — TVL variations of tissues and organs across photon energies using EGSnrc and XCOM

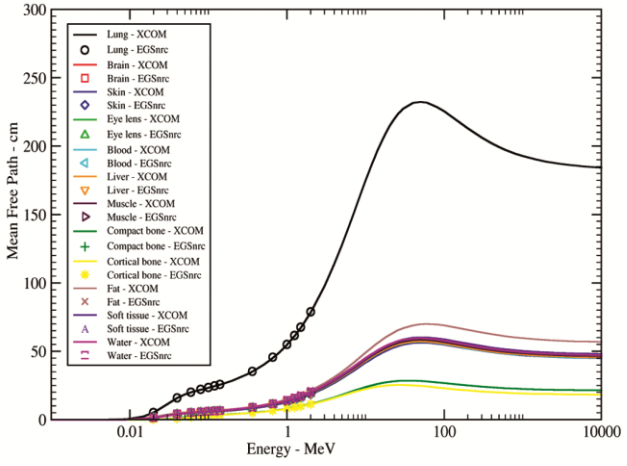

Fig. 5 — MFP variations of tissues and organs across photon energies using EGSnrc and XCOM

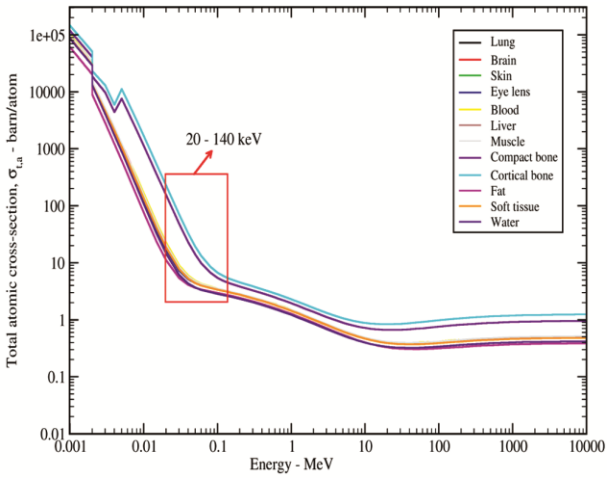

Fig. 6 — Total atomic cross-section variations with photon energy for tissue and organs

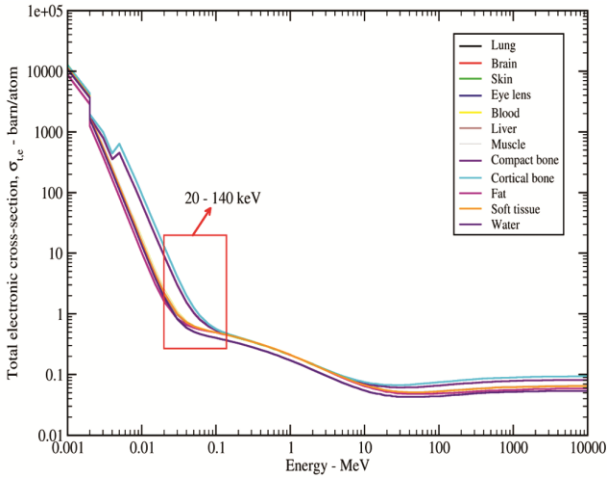

Fig. 7 — Total electronic cross-section variations with photon energy for tissue and organs

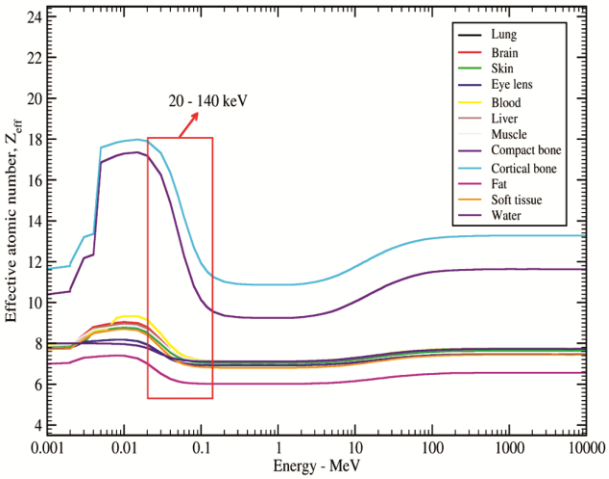

Fig. 8 — Effective atomic number variations with photon energy for tissue and organs

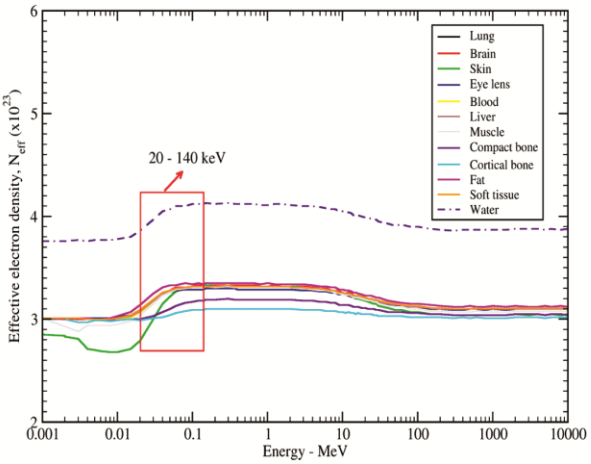

Fig. 9 — Effective electron density variations with photon energy for tissue and organs

includes photon energies emitted by computed tomography devices. It is well known that absorption properties in this energy range are primarily governed by the photoelectric effect, which is strongly influenced by the atomic number of the material's constituent elements. Therefore, the distinctions in photon absorption characteristics among various tissues and organs are more pronounced within this energy interval. As previously noted, the mass attenuation coefficient is a critical quantity for differentiating tissues and organs in terms of photon absorption, independent of their density.

Table 2 shows that the mass and linear attenuation coefficients for soft tissue, calculated using EGSnrc and XCOM, differ by less than 1%.The t-test value of 0.0032 and p-value of 0.9974 indicate that the results are statistically similar, with the differences not being significant. These findings support the reliability and consistency of both methods. In this table, the mass attenuation coefficients of soft tissue are also compared with other study results found in literature, corresponding to the same energy values.In addition, the mass attenuation coefficients data of skin calculated by this study and some other studies made by authors using different Monte Carlo simulation toolkit were given in Table 3. When looking at the data given in Table 3, it is understood that the mass attenuation coefficients calculated for skin at the same energies have values close to each other. In this study, unlike others, absorption parameters for numerous tissues and organs were calculated using the EGSnrc code. The minor differences between the results of this study and those obtained with other simulation codes can most likely be attributed to parameters such

Table 3 — The mass attenuation coefficients of skin calculated using EGSnrc in this study, and available data made some other authors in literature.

Energy (MeV)	*This study*	*Tekin et al.* [5]	*Tekin et al.* [5]	*Darki et al.* [11]	*Darki et al.* [11]	*Hamideen et al.* [12]
	EGSnrc	MCNPX	FLUKA	MCNPX	GEANT4	XCOM
0.020	0.6486			0.6982	0.6985	0.0666
0.040	0.2321					0.2330
0.060	0.1888	0.2021	0.2011			0.1890
0.080	0.1731	0.1811	0.1802			0.1730
0.100	0.1634					
0.120	0.1556					
0.140	0.1497			0.1545	0.1631	
0.364	0.1087					
0.662	0.0852					0.0848
1.000	0.0700	0.0704	0.0707			
1.250	0.0624	0.0629	0.0625	0.0615	0.0626	
1.500	0.0570	0.0571	0.0572			0.0569
2.000	0.0489	0.0491	0.0487			

Table 4 — HVL (Half-Value Layer), TVL (Tenth-Value Layer), and MFP (Mean Free Path) values of soft tissue within a specific photon energy range.

No	Energy (MeV)	HVL (cm)		TVL (cm)		MFP (cm)	
		EGSnrc	XCOM	EGSnrc	XCOM	EGSnrc	XCOM
1	0.020	0.991	0.992	3.292	3.297	1.430	1.432
2	0.040	2.844	2.862	9.451	9.509	4.104	4.130
3	0.060	3.525	3.537	11.713	11.754	5.087	5.104
4	0.080	3.863	3.860	12.835	12.826	5.574	5.570
5	0.100	4.103	4.095	13.632	13.606	5.920	5.909
6	0.120	4.313	4.296	14.331	14.275	6.224	6.200
7	0.140	4.468	4.482	14.846	14.894	6.447	6.468
8	0.364	6.180	6.173	20.535	20.509	8.918	8.907
9	0.662	7.918	7.910	26.309	26.282	11.426	11.414
10	1.000	9.556	9.586	31.751	31.850	13.789	13.832
11	1.250	10.739	10.717	35.682	35.609	15.496	15.465
12	1.500	11.780	11.775	39.140	39.124	16.998	16.991
13	2.000	13.743	13.714	45.663	45.567	19.831	19.790

t-test :0.0012 p-value: 0.999 (0.001: << 0.05)

as the number of photons used in the simulation, phantom geometry, and material input.

In this study, the half-value layer (HVL), tenth-value layer (TVL), and mean free path (MFP) values of the investigated samples were derived from their linear attenuation coefficients. The results of these quantities, specifically for soft tissue among the investigated tissues and organs, are given in Table 4.

Overall, the data in Table 4 shows that the HVL, TVL, and MFP values calculated by both methods are in close agreement, with only minor differences across the photon energy range.The HVL, TVL, and MFP values for soft tissue in the X-ray energy range (20 - 140 keV) emitted from computed tomography devices vary between 0.9 to 4.5 cm, 3.3 to 14.8 cm, and 1.4 to 6.4 cm, respectively. These values will also vary across all tissue and organs due to their different density values. Therefore, the obtained variations of HVL, TVL, and MFP values for all investigated tissues and organs were shown in Fig. 3 – 5, respectively.

Although the data were calculated across a wide photon energy range, this study primarily focuses on variations within the X-ray range emitted from CT devices. Upon analyzing these graphs, significant differences were observed for bone, fat, and lung tissue, while other tissue and organ materials showed almost identical results in all energies. These similar results for the tissues and organs are attributed to their nearly identical density values.

Table 5 presents the total atomic cross-section ($\sigma_{t,a}$), total electronic cross-section ($\sigma_{t,e}$), effective atomic number (Z_{eff}), and effective electron density (N_{eff}) values for soft tissue, calculated using EGSnrc, within the photon energy range of 0.020 – 5.0 MeV.

Table 5 — The calculated values of $\sigma_{t,a}$, $\sigma_{t,e}$, Z_{eff} and N_{eff} values for soft tissue.

Energy (MeV)	$\sigma_{t,a}$ (barn/atom)	$\sigma_{t,e}$ (barn/atom)	Z_{eff}	N_{eff} ($\times 10^{23}$)
0.020	18.462	2.195	8.412	3.089
0.030	7.753	0.996	7.783	3.190
0.040	5.294	0.722	7.335	3.258
0.050	4.435	0.625	7.101	3.284
0.060	4.019	0.576	6.976	3.301
0.080	3.619	0.526	6.876	3.312
0.100	3.386	0.495	6.838	3.318
0.120	3.218	0.472	6.825	3.321
0.140	3.083	0.452	6.816	3.318
0.364	2.235	0.328	6.807	3.320
0.662	1.744	0.256	6.807	3.320
1.250	1.287	0.189	6.806	3.320
2.000	1.008	0.148	6.814	3.317
3.000	0.812	0.119	6.832	3.310
4.000	0.699	0.102	6.851	3.304
5.000	0.626	0.091	6.874	3.295

Figs 6-9 show a graphical representation of $\sigma_{t,a}$, $\sigma_{t,e}$, Z_{eff} and N_{eff} variations of the all investigated tissue and organs, respectively. These figures are based on XCOM data, as there is no noticiable difference between the results calculated with EGSnrc and XCOM results.The variations of these quantities with photon energy across different tissues and organs are displayed across broad energy range. The CT X-ray energy range is highlighted by a red rectangular region in each graph.

The rectangular regions shown in Figs. 6-9 indicate the X-ray energy range emitted in CT devices. The total atomic and electronic cross-section variations show similar behavior to that seen in the mass attenuation coefficients,while differences between tissues and organs become more apparent when investigating the variations of the effective electron density and effective atomic number values. It is seen from the Fig. 8 that bone tissues exhibit higher effective atomic numbers (Z_{eff}) compared to other tissues and organs. Z_{eff} values of the investigated samples increase between 1-3 keV and remain nearly constant from 3-20 keV. A sharp decline is observed for Z_{eff} values between 20-100 keV, where the photoelectric effect is the dominant interaction type. As a result, the Z_{eff} values of all tissues and organs are comparable in this energy range. From 100 keV to 10 MeV, Z_{eff} values remain stable across all tissues and organs, as incoherent scattering and pair production become dominant interactions. At higher energy levels, where photonuclear reactions are likely to occur, Z_{eff} increases slightly and then remains constant.

As shown in Fig. 9, the effective electron density for water is considerably higher compared with the other tissues and organs. This reveal that why water or water-like materials scatter more radiation than denser substances. This may be attributed to the number of atom and electron per unit volume.

This study comprehensively presents all radiation absorption quantities for 11 different tissues/organs and water medium in detail across a broad photon energy range. Specifically, the primary focus of this study is to comprehensively determine and analyze the absorption quantities for various tissues and organs over the spectrum of X-ray energies used in CT imaging. The photon absorption quantities in the rectangular region shown in Figs. 6-8 demonstrate greater variability among tissues and organs compared to other photon energy ranges. Consequently, it is evident that the radiation absorption effects of tissues and organs within this energy range, emitted from CT devices, will also exhibit distinct characteristics.

3.2 Dosimetric cal culations

In simulations conducted to analyze dosimetric variations, the user code *'dosrznrc'* from the EGSnrc platform was employed. This code enables calculation of the radiation dose deposited within a cylindrical medium as a function of depth. The image in Fig. 10 presents the semi-cylindrical section of the cylindrical phantom utilized in these calculations. In this setup, ionizing photons of specified energy traverse the medium until their energy is fully depleted and absorbed. This process results in depth-dependent radiation dose deposition within the medium. The deposited radiation dose is influenced by the photon

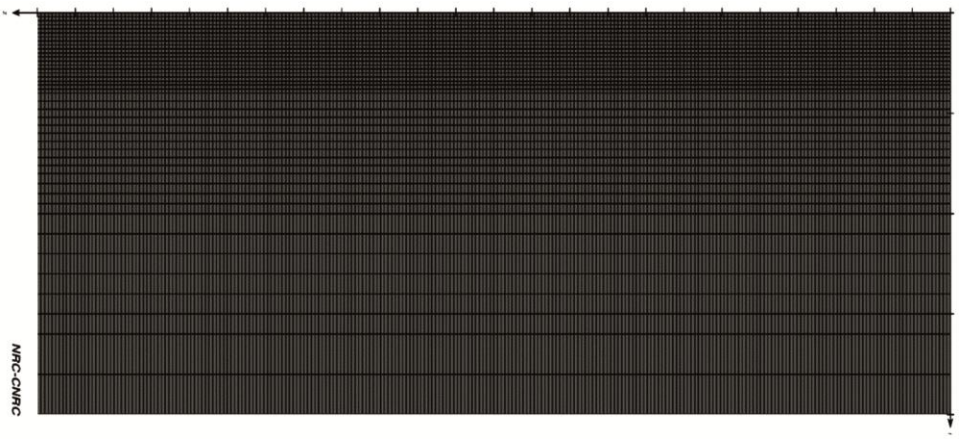

Fig. 10 — Semi-cylindrical image of the phantom with voxelized geometry

energy, its intensity, and the type of medium. Hence, determining the variation in dose values deposited by radiation within specific tissues or organs is crucial for understanding their absorption characteristics and potential impacts.

During the modeling of the cylindrical geometry in data input file, the points where the dose values would be absorbed were determined as shown in Fig. 10. In this geometry, the cylinder's length was set to 25 cm, and its radius was set to 10 cm. The long axis (z-axis) of the cylinder was divided into 1.0 mm slices. Additionally, the cylinder consists of multiple nested cylinders. The innermost cylinder, with a 2 cm radius (4 cm diameter), consists of 1.0 mm interval layers. This design ensures precise dose values, as it is the region of intense radiation absorption and the deposition point along the central axis. The region between 2.0 cm and 5.0 cm radius was modeled using nested cylinders with 2.0 mm intervals, while the intervals were increased to 5.0 mm between 5.0 cm and 8.0 cm radius, and 10.0 mm between 8.0 cm and 10.0 cm radius.

An example of a simulation performed using real tissue content within the modeled cylindrical geometry is shown in Fig. 11. In the simulations, the radiation source was positioned 5 cm in front of the cylinder, emitting a narrow beam along the cylinder's central axis in the positive z-axis direction.

Upon analyzing the graphs in Figs. 3-5, which illustrate the calculated HVL, TVL, and MFP quantities, significant differences are observed in the results for lung, bone, and fat tissues compared to the other tissues investigated in this study. Based on these findings, the dosimetric calculations in this study were carried out for cortical bone, lung, and liver. Cortical bone represents the highest density tissue in the human body, while lung represents the lowest density organ. Since the densities of all other tissues and organs are similar, the liver was chosen as a representative tissue among them. The dose variations with depth in the modeled cylindrical phantom, for the X-ray energy range emitted from the CT device, are shown in Figs. 12-14.

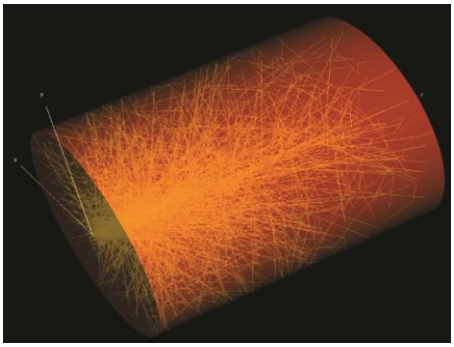

Fig. 11 — An illustration of a simulation performed for dosimetric calculations

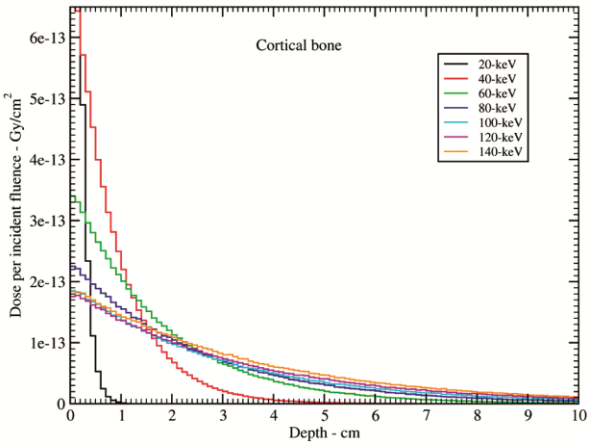

Fig. 12 — The depth-dependent absorbed dose variations for cortical bone at photon energies emitted from CT device

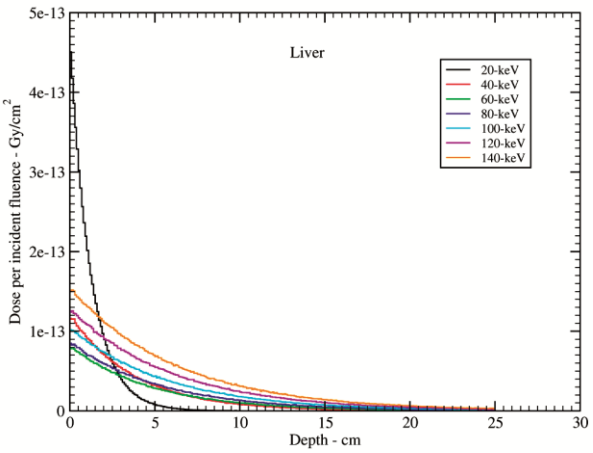

Fig. 13 — The depth-dependent absorbed dose variations for liver at photon energies emitted from CT device

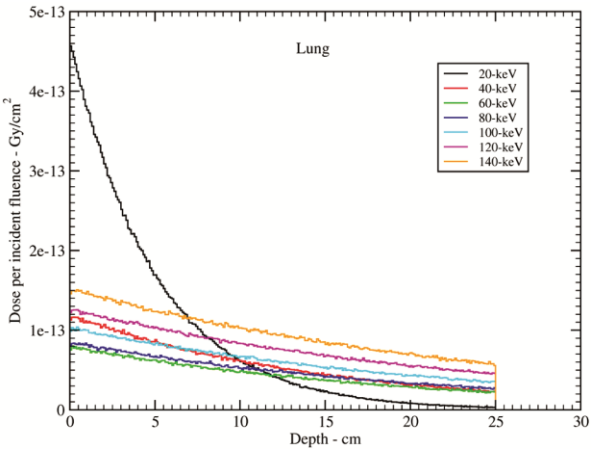

Fig. 14 — The depth-dependent absorbed dose variations for lung at photon energies emitted from CT device

When investigating the depth-dependent dose variation graphs, it is observed that photons with a maximum energy of 140 keV emitted from the CT device can travel up to 10 cm within cortical bone material, while lower-energy photons are completely absorbed over shorter distances. According to the simulation results, photons with a maximum energy of 140 keV are nearly completely absorbed within 25 cm in the liver, but a very small amount of dose is deposited slightly beyond 25 cm. In a study conducted by increasing the phantom size used in the simulation, it was determined that no dose was recorded in the lung tissue beyond a distance of 30 cm. The decrease in dose values with depth depends on both the photon energy and the tissue composition. The comparison of the simulation results for the depth-dependent dose variations in bone, liver, and lung tissues with different density values is shown in Fig. 15, using 100 keV photons and a 25 cm-long phantom.

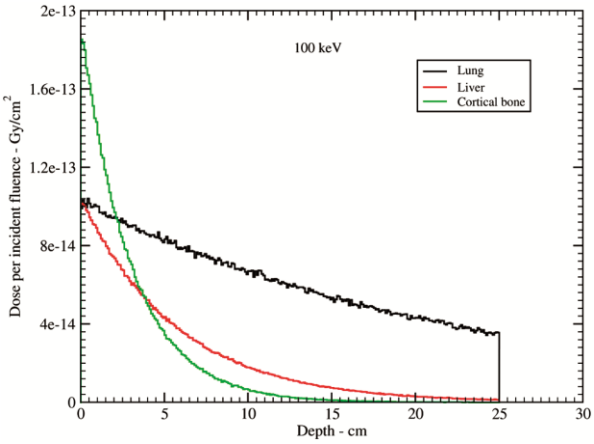

Fig. 15 — Comparison of depth-dependent dose variations obtained for 100 keV photons in cortical bone, liver, and lung phantoms

In the calculations, the radiation source, modeled to emit a parallel beam with a diameter of 0.5 mm, was aligned exactly along the central axis. Therefore, in this study, the dose variations with depth were derived from the data obtained from the voxels along the central axis of the cylindrical phantom.This is because the radiation dose absorbed in the voxels along the +z axis at the cylinder's center can be measured at the farthest distances, while X-rays are absorbed at shorter distances in voxels outside the center, depending on the radius.The simulation results, with the point source (0.5 mm) placed along the central axis of the phantom, illustrate the variations in radiation dose with depth both along the central axis and at other locations along the +z axis outside the radius. Fig. 16 presents the dose variations as a function of the radius for the soft tissueat an average photon energy of 40 keV emitted from the CT device.

The black curve in the figure illustrates the depth-dependent dose variations along the central axis of the cylinder, while the yellow curve represents the dose variations along the +z direction at a point 4 mm radially outward from the center. The figure shows that the maximum depth at which dose values are recorded was obtained along the central axis. As the point moves radially outward, the absorbed dose along each +z direction decreases progressively with increasing radial distance. The dose is absorbed over the shortest depth along the +z direction at the outermost point (4 mm), as indicated by the yellow curve. This pattern is consistent across other photon energies as well. In simulations analyzing depth-dependent dose variations, the point radiation source was positioned 5 cm in front of the center of the

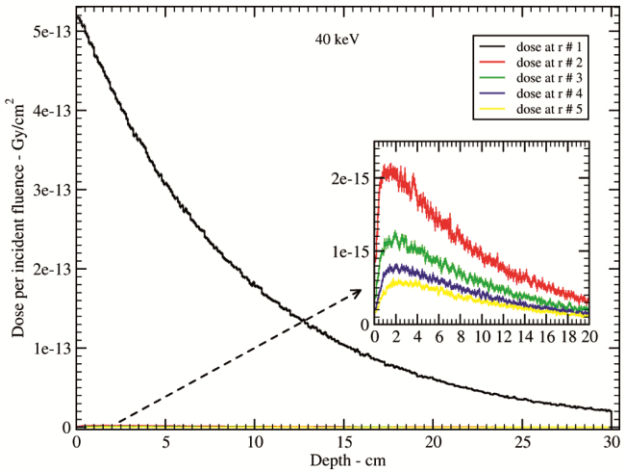

Fig. 16 — Depth-dependent dose variations along the central axis (black curve) and along the +z direction at increasing radial distances outward from the origin for photons with an energy of 40 keV in a soft tissue phantom. Here, r#1, r#2, r#3, r#4, and r#5 represent the +z directions located at radial distances of 0, 1, 2, 3, and 4 mm from the center, respectively

circular surface facing the phantom's long axis, as shown in Fig. 11. The points where dose readings were taken at the farthest distances are along the central axis of the cylinder, as also shown in Fig. 16. Therefore, only the dose values obtained along the central axis of the cylinder were considered in this study.

4 Conclusion

This study comprehensively investigates the radiation absorption properties of 11 different human tissues/organs and a water medium across a broad photon energy range, using the EGSnrc Monte Carlo code. Key radiation absorption quantities, including the mass attenuation coefficient (μ_m), linear attenuation coefficient (μ), total atomic cross-section ($\sigma_{t,a}$), total electronic cross-section ($\sigma_{t,e}$), effective atomic number (Z_{eff}), effective electron density (N_{eff}), half-value layer (HVL), tenth-value layer (TVL), and mean free path (MFP), were determined. These quantities were specifically analyzed for their relevance to the X-ray spectrum emitted by CT devices, and the results were compared to those obtained from the NIST XCOM database and other studies found in the literature. Our findings show strong agreement with these sources, reinforcing the reliability of the calculated results.

A key observation is the significant variations in radiation absorption quantities across the studied tissues and organs, particularly within the CT X-ray energy range. These variations are mainly attributed to differences in tissue density and atomic composition. Notably, the mass attenuation coefficient, a critical parameter, allows for comparisons across tissues and organs regardless of their density, providing useful insights for medical physicists evaluating radiation behavior in different tissues.

Furthermore, the study emphasizes the importance of the calculated HVL, TVL, and MFP values for human tissues, which are crucial for understanding photon penetration in medical imaging and radiation therapy. These quantities provide valuable data for healthcare professionals, helping optimize the balance between image quality and radiation dose. The variations in these values influence radiological risk assessments and enhance planning for radiotherapy treatments.

In addition to these findings, the study explores how radiation dose deposition varies with tissue depth. This aspect is essential for optimizing dose constraints in radiotherapy and minimizing unnecessary radiation exposure to healthy tissues. The data on dose variations, derived from different tissues and organs, provide actionable insights for improving patient safety in clinical settings and guiding the development of more efficient treatment protocols. Moving forward, future research could focus on refining dose modeling techniques for specific clinical applications, including pediatric imaging and personalized radiotherapy. The implications of this study extend beyond the medical imaging community, as it contributes to advancements in radiation protection and radiotherapy optimization.

In conclusion, this study highlights the significance of understanding tissue-specific radiation absorption properties, particularly in the CT X-ray energy range. The findings offer critical insights for medical physicists and healthcare professionals to enhance radiation safety, improve diagnostic imaging protocols, and optimize radiotherapy treatment planning. Further investigation into tissue-specific radiation dose distributions and their relationship to clinical outcomes will continue to shape future advancements in radiation medicine.

Acknowledgements

We would like to express our sincere gratitude to Ondokuz Mayıs University, Graduate Schools, for its invaluable support and for providing the resources and academic environment that made this research possible.

References

1 Manjunatha H C, *J Med Phys*, 39 (2014) 112.
2 Hermosilla A, Londono G D, Garcia M, Ruiz F, Andrade P & Perez A, *Radiat Prot Dosimetry*, 162 (2014) 508.
3 Trunova V, Sidorina A & Kriventsov A, *Appl Radiat Isot*, 95 (2015) 48.
4 Ermis E E, Pilicer F B, Pilicer E & Celiktas C, *Nucl Sci Tech*, 27 (2016) 1.
5 Tekin H O, Singh V P, Altunsoy E E, Manici T & Sayyed M I, *Iran J Med Phys*, 14 (2017) 229.
6 Arslan H, *Nucl Sci Tech*, 30 (2019) 1.
7 Joshi S, Ajikumar P K, Sivasubramanian K & Jayaraman V, *J Polym Eng*, 40 (2020) 99.
8 Al-Buriahi M S, Arslan H & Tonguç B T, *Indian J Pure Appl Phys*, 57 (2019) 433.
9 Moradi F, Khandaker M U, Alrefae T, Ramazanian H & Bradley D A, *Appl Radiat Isot*, 146 (2019) 120.
10 Saleh H H, Sharaf J M, Alkhateeb S B & Hamideen M S, *Radiat Phys Chem*, 165 (2019) 108388.
11 Darki S Y & Keshavarz S, *Nucl Sci Tech*, 31 (2020) 119.
12 Hamideen M S, Abady R S & Sharaf J M, *Latv J Phys Tech Sci*, 59 (2022) 64.
13 Islam S, Mahmoud K A, Sayyed M I, Alim B, Rahman M & Mollah A S, *Radiat Phys Chem*, 172 (20200 108559.
14 Kadri O & Alfuraih A, *Appl Sci*, 12 (2022) 4250.
15 Rafiei M M, Parsaei S, Kaur P, Singh K J, Büyükyıldız M & Kurudirek M, *Biomed Phys Eng Expr*, 8 (2022) 025002.
16 Esien-Umo E O, Obu J A, Chiaghanam N O, Ugbem T I & Egbe N O, *J Med Phys*, 47 (2022) 381.
17 Üncü Y A, Sevim G, Ağar O & Özdoğan H, *Kuwait J Sci*, 50 (2023) 1A.
18 Shivaramu, *Med Dosim*, 27 (2002) 1.
19 Manjunatha H C & Rudraswamy B, *Health Phys*, 104 (2013) 158.
20 Kurudirek M, *Radiat Phys Chem*, 102 (2014) 139.
21 Gobo M S, Soares L D H & Poletti M E, *Radiat Phys Chem*, 167 (2020) 108260.
22 Manohara S R, Hanagodimath S M & Gerward L, *J Appl Clin Med Phys*, 12 (2011) 296.
23 Jarrah I, Radaideh M I & Kozlowski T, *Radiat Phys Chem*, 160 (2019) 15.
24 Salehi D, Sardari D & Jozani M S, *J Radiat Res Appl Sci*, 8 (2015) 439.
25 Rafiei M M, Tavakoli-Anbaran H & Kurudirek M, *Radiat Phys Chem*, 177 (2020) 109118.
26 Saleh H H, Sharaf J M & Abady R S, *Appl Radiat Isot*, 167 (2021) 109464.
27 Joshi S, Rao J S B, Sivasubramanian K & Kumar R, *J Polym Res*, 24 (2017) 1.
28 Anugrah M A, Suryani S, Ilyas S, Mutmainna I, Fahri A N, *et al*., *Radiat Phys Chem*, 173 (2020), 108878.
29 Zhou H, Keall P J & Graves E E, *Med Phys*, 36 (2009) 1008.
30 Böke A, *Chin J Phys*, *55* (2017) 2165.
31 Kawrakow I, Rogers D W O, Mainegra-Hing E Tessier, F, Townson R W & Walters B R B, EGSnrc toolkit for Monte Carlo simulation of ionizing radiation transport, 2000.
32 Berger M J, Hubbell J H, Seltzer S M, Chang J, Coursey J S, Sukumar R, et al., XCOM Photon Cross Sections Database, NIST, PML, *Radiat Phys Div*, 2010.
33 Mayles P, Nahum A & Rosenwald J C, Handbook of radiotherapy physics: theory and practice, CRC Press, 2007.
34 Knoll G F, Radiation detection and measurement, John Wiley & Sons, 2010.
35 Gülbiçim H, Tufan M C & Turkan M N, *Radiat Phy Chem*, 130 (2017) 112.
36 Scott J A, Photon, electron, proton and neutron interaction data for body tissues: ICRU report 46. International commission on radiation units and measurements, Technical Report, Bethesda, 1992.
37 Woodard H Q & White D R, *BR J Radiol*, 59 (1986) 1209.